Published in final edited form as:

Cancer Res. 2020 October 15; 80(20): 4371–4385. doi:10.1158/0008-5472.CAN-20-0458.

EZH2-mediated Downregulation of the Tumor Suppressor DAB2IP Maintains Ovarian Cancer Stem Cells

Xingyue Zong[1], **Weini Wang**[1], **Ali Ozes**[1], **Fang Fang**[1], **George E. Sandusky**[2], **Kenneth P. Nephew**[1,3,4,*]

[1]Medical Sciences, Indiana University School of Medicine, Bloomington, IN, USA

[2]Department of Pathology and Laboratory Medicine, Indiana University School of Medicine, Indianapolis, IN, USA

[3]Melvin and Bren Simon Comprehensive Cancer Center, Indiana University, Indianapolis, IN, USA

[4]Department of Anatomy, Cell Biology and Physiology, Indiana University School of Medicine, Indianapolis, IN, USA

Abstract

The majority of women diagnosed with epithelial ovarian cancer (OC) eventually develop recurrence which rapidly evolves into chemoresistant disease. Persistence of ovarian cancer stem cells (OCSC) at the end of therapy may be responsible for emergence of resistant tumors. In this study, we demonstrate that in OCSC, the tumor suppressor Disabled Homolog 2-Interacting Protein (DAB2IP) is silenced by EZH2-mediated H3K27 trimethylation of the DAB2IP promoter. CRISPR/Cas9-mediated deletion of DAB2IP in epithelial OC cell lines upregulated expression of stemness-related genes and induced conversion of non-CSC to CSC, while enforced expression of DAB2IP suppressed CSC properties. Transcriptomic analysis showed that overexpression of DAB2IP in OC significantly altered stemness-associated genes and bioinformatic analysis revealed WNT signaling as a dominant pathway mediating the CSC inhibitory effect of DAB2IP. Specifically, DAB2IP inhibited WNT signaling via downregulation of WNT5B, an important stemness inducer. Reverse Phase Protein Array further demonstrated activation of non-canonical WNT signaling via C-JUN as a downstream target of WNT5B, which was blocked by inhibiting RAC1, a prominent regulator of C-JUN activation. Co-administration of EZH2 inhibitor GSK126 and RAC1 inhibitor NSC23766 suppressed OCSC survival in vitro and inhibited tumor growth and increased platinum sensitivity in vivo. Overall, these data establish that DAB2IP suppresses the cancer stem cell phenotype via inhibition of WNT5B-induced activation of C-JUN and can be epigenetically silenced by EZH2 in OCSC. Targeting the EZH2/DAB2IP/C-JUN axis therefore presents a promising strategy to prevent OC recurrence and has potential for clinical translation.

Keywords

ovarian cancer; epigenetics; cancer stem cells; tumor suppressor gene; chemoresistance

[*]**Corresponding Author:** Kenneth P. Nephew, PhD, Medical Sciences Program, Indiana University School of Medicine, Jordan Hall 302; 1001 East Third Street, Bloomington, IN 47405, knephew@indiana.edu.

Disclaimers: none; no conflicts of interest to disclose.

Introduction

Ovarian cancer (OC) is a chemoresponsive tumor with very high initial response rates to standard therapy consisting of platinum/paclitaxel. However, about 75% of women diagnosed with advanced stage high-grade serous (HGS) OC experience chemoresistant relapse after first-line chemotherapy and have a five-year survival rate of only 26% (1,2). Recurrent OC is essentially incurable. There is an urgent need to develop strategies and novel approaches to improve the clinical outcome for OC patients.

Although chemotherapy initially decreases tumor bulk, it may leave behind residual cancer stem cells (CSCs) capable of regenerating tumors (3). Persistence of ovarian cancer stem cells (OCSCs) at the end of therapy has been shown to be a key contributor to resistant tumors (4). CSC possess properties such as a quiescent state, increased ABC transporter efflux and enhanced DNA damage response, rendering them ‘undruggable’ by traditional cytotoxic interventions (5). Analogous to normal stem cells, CSC maintenance requires elaborate orchestration of the epigenome, and aberrant epigenetic alterations are common features of CSC, including OCSC (6–8), which may represent therapeutic vulnerabilities. Thus, it is of great interest to understand the (epi)genetic mechanism responsible for OCSC survival and develop strategies to target these recalcitrant cells.

Disabled Homolog 2-Interacting Protein (DAB2IP) is a tumor suppressor frequently down-regulated in multiple aggressive cancers (9,10). In addition to possessing Ras-GTPase activity, DAB2IP serves as a multi-functional scaffold protein, and DAB2IP loss affects multiple oncogenic signaling pathways (9,10). Recent studies in renal, prostate and colorectal cancer demonstrated that DAB2IP expression inhibited CSC-like phenotypes, suggesting a role for DAB2IP in suppressing CSCs (11–13). Epigenetic silencing of DAB2IP by EZH2, the enzymatic subunit of the polycomb repressive complex 2 (PRC2), was reported in medulloblastoma (14) and prostate (15) cancers but whether EZH2 regulates DAB2IP regulation in CSC has not been examined.

In this study, with the goal of identifying new therapeutic targets of OCSCs to inhibit tumor relapse and overcome chemoresistance, we demonstrate that combining an epigenetic therapy with a non-canonical WNT signaling pathway has the potential to eliminate OCSCs. We show that DAB2IP was downregulated in OCSCs and could be derepressed by inhibiting EZH2-induced H3K27 trimethylation. By using transcriptomic (RNA-seq) analysis combined with reverse phase protein array (RPPA), we establish that downregulation of DAB2IP enriched OCSC by promoting WNT5B-induced C-JUN activation in the non-canonical wingless-related integration site / planar cell polarity (WNT/PCP) pathway. Furthermore, preventing epigenetic-mediated silencing of DAB2IP with an EZH2 inhibitor and blocking WNT5B-induced non-canonical WNT signaling using a RAC1 inhibitor synergistically repressed OCSC survival *in vitro* and enhanced platinum sensitivity in a mouse xenograft model. We suggest that combining an epigenetic therapy with a non-canonical WNT pathway signaling pathway inhibitor may be required to eradicate ovarian cancer stem cells. We propose this promising strategy to prevent OC recurrence has potential for clinical translation.

Materials and Methods

Cell culture.

OC cell lines OVCAR3 and A2780 were obtained from the American Type Culture Collection (ATCC, Manassas, VA); COV362 was obtained from Sigma. These cell lines were authenticated by short tandem repeat (STR) analysis in 2017 (IDEXX BioAnalytics, Columbia, MO). Kuramochi cell line was obtained from the Japanese Collection of Research Bioresources and authenticated by short tandem repeat (STR) analysis in 2018 (Clinical Molecular Oncology Laboratory, University of Kansas Cancer Center, KS). Cells were cultured as we have described previously (16). Cell lines were tested for mycoplasma contamination (Lonza) every 6 months. See Supplementary Material (SM) for more information.

Immunofluorescence and immunohistochemistry (IHC).

For Immunofluoresence staining, OC cells were fixed, permeabilized and stained (17). At least 3 random images from 3 independent experiments were taken using a light microscope. For IHC, OC tissue microarray OVC481 was purchased from Pantomics. See SM for a detailed description.

Flow cytometry.

ALDH enzymatic activity was measured using the AldeRed ALDH Detection Assay kit (Millipore) or Aldefluor assay kit (Stem Cell Technologies) following the manufacturer's instructions. ALDH (+) cells were determined by FACS Aria II flow cytometer (BD Biosciences) or LSRII flow cytometer (BD Biosciences). Diethylamino benzaldehyde (DEAB) was added to each sample and served as a negative control for gating purpose as we have described (8). For CD133 detection, 1 million cells were harvested and incubated 50:1 with CD133/1-PE-Vio615 antibody or REA Control Antibody (Miltenyi Biotec) for 10min in the dark at 4 °C. Cells were washed with ice-cold PBS and filtered before subjected to flow cytometry analysis. Data was collected with FACSDiva software (BD Biosciences) and analyzed with FlowJo software (FlowJo LLC).

Tumorsphere assay.

Briefly, monolayer culture cells were trypsinized, and 500 or 1000 cells were seeded into ultra-low attachment plates (Corning). Cells were cultured for indicated days, observed and counted using a Zeiss Axiovert 40 inverted microscope with Axio-Vision software as we have described (8,18). See SM for a detailed description.

CRISPR/Cas9.

OC cells were co-transfected with DAB2IP CRISPR/Cas9 KO (sc-406961-KO-2) and DAB2IP HDR (sc-406961-HDR-2), or control CRISPR/Cas9 (sc-418922) plasmids from Santa Cruz using UltraCruz® transfection reagent (sc-395739) and plasmid transfection medium (ssc-108062) according to manufacturer's protocol. DAB2IP CRISPR/Cas9 KO plasmid consists of a pool of 3 plasmids designed to disrupt gene expression by causing a double-strand break in exons within the DAB2IP gene, while the control CRISPR/Cas9

plasmid contains a non-targeting 20nt scramble guide RNA (gRNA). Selection procedure for stably transfected clones is described in SM.

Immunoblotting.

Cell lysates were prepared with RIPA lysis buffer (Thermo Fisher) containing Pierce™ protease inhibitor cocktails and Pierce™ phosphatase inhibitor. See SM for a detailed description.

Chromatin immunoprecipitation (ChIP) and real-time qPCR.

See SM for a detailed description. Primer sequences were listed in Supplementary Table S1 and S2.

MTT and migration assay.

For MTT, 2000 cells were seeded in 96-well plates in triplicates and allowed to grow for 1 day. IC_{50} values were calculated using Prism 6 (GraphPad Software). For migration assay, a total of 200,000 cells were seeded inside migration Boyden chamber inserts (8 mm pore; Corning) in serum free media supplemented with 0.1% BSA as we have described (19). See SM for detailed descriptions of these assays.

RNA-sequencing analysis.

RNA-seq was performed essentially as we have described (19,20). Biological triplicates of OVCAR3 cells transfected with DAB2IP overexpressing vector and empty vector were lysed with RLT, and RNA was extracted with RNeasy Mini kit (Qiagen) according to the manufacturer's protocol. The RNA-sequencing results are available for download at Gene Expression Omnibus (GEO) data repository at the National Center for Biotechnology Information (NCBI) under the accession number GSE144948. See SM for a detailed description and bioinformatic analysis.

Reverse Phase Protein Array (RPPA).

OVCAR3-DAB2IP overexpressing cells with or without recombinant WNT5B-treatment, as well as empty vector control cells, were washed twice in ice-cold PBS and harvested (three biological replicates per sample). Samples were sent to the RPPA Core Facility at MD Anderson Cancer Center for further analysis. See SM for analysis results and bioinformatic analysis.

Cell transfection and plasmids.

For EZH2 knockdown, cell lines were transfected with two independent lentivirus-based shRNAs (MISSION® shRNA, Sigma Aldrich) targeting human EZH2 gene. Sequence of shEZH2s can be found in SM.

Mouse xenograft experiments.

All animal studies were conducted according to ethical guidelines approved by the Institutional Animal Care and Use Committee of Indiana University. 2×10^6 OVCAR3 cells were mixed with matrigel at 1:1 ratio and injected subcutaneously into right flanks of NOD/

SCID 5-week-old female mice (Envigo). Tumor size was measured twice a week with a caliper, and tumor volume was determined using the formula $V=½ \times L \times W^2$. When average tumor volumes reached $100mm^3$, mice were randomized into eight groups (N=6 mice per group), and corresponding treatment was initiated by i.p. injection. Xenograft tumors were collected at the end of study, followed by tumor dissociation procedures. Single-cell suspension were obtained using tumor dissociation kit (Miltenyi Biotec) in combination with the gentleMACS™ Dissociator, prior to flow cytometry analysis. Establishment of Kuramochi xenograft model can be found in SM.

Statistical analysis.

All data are presented as mean values ± SD of at least three biological experiments unless otherwise indicated. The estimate variation within each group was similar therefore student's t-test was used to statistically analyze the significant difference among different groups. Combination Index (CI) was determined as previously reported (21) and see SM for more details.

Results

DAB2IP is downregulated in ovarian cancer (OC) patients and correlates with poor patient survival

DAB2IP has been shown to play a key role in tumor growth inhibition in multiple types of aggressive cancers, including prostate and colorectal cancer (9). To determine whether DAB2IP is a tumor suppressor in OC, we queried publicly available databases, including gene expression profiles in The Cancer Genome Atlas (TCGA) data portal. DAB2IP expression in ovarian tumor samples was lower compared to paired normal tissues using Gene Expression Profiling Interactive Analysis of the TCGA (Fig. 1A). A similar downregulated expression pattern was observed in several cancers, compared to corresponding normal tissues (Supplementary Fig. S1A). To determine whether DAB2IP contributes to OC disease progression, Ovarian Cancer Database of Cancer Science Institute Singapore (CSIOVDB) (22) was analyzed. Low DAB2IP expression correlated with poor disease-free survival rate (n=707, p=0.0105) and high-grade disease (Fig. 1B and Supplementary Fig. S1B). In addition, differential expression of DAB2IP was observed across OC histological subtypes, with significantly lower (p=8.77e-12) DAB2IP expression in high-grade serous OC compared to low malignant potential (LMP) serous OC (Supplementary Fig. S1C). Taken together, these results indicated that DAB2IP negatively correlated with disease progression and that low DAB2IP level was associated with poor prognosis of OC.

Inverse correlation of DAB2IP and EZH2 in OC tumors and cell lines

As DAB2IP inactivation due to EZH2-mediated H3K27 methylation has been reported (14,15), it was of interest to investigate whether DAB2IP was associated with EZH2 transcriptional silencing in patient tumors. Analysis of transcriptomic profiles of 308 OC tumors from TCGA data portal showed an inverse correlation between EZH2 and DAB2IP expression (Fig. 1C). Furthermore, protein expression of DAB2IP and EZH2 by immunohistochemical (IHC) analysis of an OC tissue microarray demonstrated a significant

inverse correlation (r= −0.37, p<0.05) between DAB2IP and EZH2 (Fig. 1D, E). Expression of EZH2 in OC patients with different subtypes and disease grades was analyzed. Greater expression of EZH2 in high-grade disease was observed, with DAB2IP showing the opposite expression pattern (Supplementary Fig. S1B, D). In contrast to DAB2IP, EZH2 demonstrated significantly higher (p=5.65e-18) expression in high-grade serous OC compared to the serous subtype of LMP OC (Supplementary Fig. S1E). Based on the above observation in patients OC tumor data, it was of interest to investigate whether EZH2 negatively regulated expression of DAB2IP in OC cell models. EZH2 knockdown increased DAB2IP expression compared to empty vector transfected cells at both mRNA and protein levels (Supplementary Fig. S1F and G). Furthermore, we examined H3K27me3 occupancy on the DAB2IP promoter by using four different primer sets spanning 2kb upstream of the DAB2IP transcription start site (TSS) and chromatin immunoprecipitation (ChIP) analysis followed by qPCR. H3K27me3 occupancy at the DAB2IP promoter was significantly reduced after EZH2 knockdown (Supplementary Fig. S2A, B). Collectively, the data indicated that DAB2IP was regulated by EZH2 in OC and the inverse relationship was associated with patient outcomes.

DAB2IP is downregulated by EZH2 in OCSCs

Persistence of CSCs and disease progression have been reported in experimental models of OC and in patient tumors (23,24). We next tested whether downregulation of DAB2IP was associated with OCSC phenotypes. ALDH, a well-accepted CSC marker, was used to isolate OCSCs in our study due to its enhanced ability to initiate tumor growth as previously reported (8,25–27). Subpopulations of CSC and non-CSC were isolated by fluorescence-activated cell sorting (FACS), based on ALDH activity from OC cell lines Kuramochi, OVCAR3, COV362 and A2780. We first confirmed that the ALDH(+) subpopulation of different OC cell lines was enriched for expression of stemness-related genes, including TWIST, NANOG, OCT4 and PROM1 (Supplementary Fig. S2C) and then investigated whether DAB2IP played a role in regulating ALDH(+) OCSCs. Expression of DAB2IP in ALDH(+) cells was significantly lower compared to non-CSC ALDH(−) cells at both mRNA and protein levels (Fig. 1F, G), indicating that DAB2IP was downregulated in OCSC population and associated with regulating stemness. Similarly, a significant increase in EZH2 expression was detected in ALDH(+) cells vs. ALDH(−) cells in three OC cell lines (OVCAR3, COV362 and A2780) (Supplementary Fig. S2D). To investigate whether the underlying mechanism of DAB2IP downregulation in OCSCs was due to EZH2-H3K27me3, we examined H3K27me3 occupancy on the DAB2IP promoter. Enrichment of H3K27me3 at DAB2IP promoter loci was greater in CSCs than non-CSCs (Fig. 1H), and knocking down EZH2 in OCSCs increased DAB2IP mRNA (Fig. 1I) and re-expressed DAB2IP protein (Fig. 1J). Overall, these findings demonstrated that downregulation of DAB2IP in OCSCs was mediated by EZH2-induced H3K27me3 at the DAB2IP promoter.

EZH2-regulated DAB2IP in OCSCs inhibits spheroid formation

Although upregulation of EZH2 in side population of cells isolated from ascites of OC patients has been reported (7), the function of EZH2 in OCSC maintenance remains incompletely understood. To explore the role of EZH2 in supporting spheroid formation ability, we first examined EZH2 levels in spheroids. Immunofluorescent staining showed

nuclear EZH2 expression in ovarian tumor spheroids (Fig. 2A, Supplementary Fig. S2E). To further assess the role of EZH2 in spheroid formation, OC cell lines were stably transfected with shRNA targeting EZH2 or with non-silencing control shRNA vector and then seeded into ultra-low attachment plates. EZH2 downregulation significantly inhibited spheroid formation (Supplementary Fig. S2F–I), demonstrating a key role for EZH2 in spheroid formation, a hallmark of the CSC phenotype. To test if decreased spheroid number was due to a change in cell proliferation, proliferation rate was assessed after EZH2 knockdown. The proliferation curve showed a 10%-20% decrease (Supplementary Fig. S3A, B), compared to an approximately 50% decrease in spheroid formation (Supplementary Fig. S2F–I), indicating a greater impact of EZH2 knockdown on reduced stemness to inhibit spheroid formation compared to a decrease in cell number.

To complement the genetic inhibition studies and explore whether the inhibitory effect was dependent on the enzymatic activity of EZH2, the selective EZH2 inhibitor GSK126 was utilized (Supplementary Fig. S3C). Treatment with sub IC_{50} concentrations of GSK126 (5 or 10 μM; IC_{50}=14 μM) disrupted spheroid formation under non-adherent conditions (Fig. 2B–D; Supplementary Fig. S3D–F). Moreover, GSK126 treatment of OC cells under non-adherent conditions resulted in decreased ALDH(+) activity based on ALDEFLUOR assay compared to negative control cells treated with DEAB (Fig. 2E, F; Supplementary Fig. S3G), supporting that enzymatic inhibition of EZH2 suppressed CSC enrichment during spheroid formation. To further explore EZH2 regulation of DAB2IP in the context of spheroid formation, DAB2IP knockdown was performed in stable EZH2 knockdown cells (Supplementary Fig. S3H). Spheroid formation ability was restored (Fig. 2G, H), indicating that DAB2IP plays a critical role as a downstream effector of EZH2 suppression of tumorsphere formation in OCSCs.

DAB2IP expression suppresses the CSC phenotype

As our findings indicated that OCSCs were deficient in DAB2IP and pointed to a previously unidentified role for DAB2IP in opposing EZH2-induced tumorsphere formation, we hypothesized that DAB2IP is a suppressor of the CSC phenotype. To test this hypothesis, we generated DAB2IP knockout (DAB2IP-KO) cells lines using CRISPR/CAS9 system (Fig. 3A). Increased expression of stemness-related genes, including OCT4, NANOG, BMI1 and PROM1, was observed in the DAB2IP-KO OVCAR3 clones (Fig. 3B). PROM1 encodes promomin-1, also known as CD133, and previous reports have demonstrated greater tumor-initiating ability in CD133(+) cells vs. CD133(−) cells isolated from primary OC tumors and cell lines (27–29). Consistent with the marked increase in PROM1 expression (Fig. 3B), the CD133(+) population, another well-accepted OCSC marker, significantly increased from 0.4% to over 20% in the DAB2IP-KO clones (Fig. 3C). In addition, enhanced tumor spheroid formation by DAB2IP-KO clones was observed (Supplementary Fig. S4A, B).

Despite increased cancer stemness properties and CD133(+) population, the ALDH(+) population was not increased by DAB2IP-KO in OVCAR3 cells (Fig. 3D), perhaps due to the relatively high basal ALDH activity in the OVCAR3 cell line. To address this possibility, DAB2IP knockout was performed in OC cell lines with low basal population of ALDH(+) cells, Kuramochi and A2780 (approximately 2% ALDH(+) cells). Enrichment of the

ALDH(+) population in DAB2IP-KO Kuramochi and A2780 cells (by 1.6 fold and 3.3 fold respectively; Fig. 3E; Supplementary Fig. S4C, D) was observed. ALDH1 protein level increased (Fig. 3F) and the CD133(+) population also increased compared to control cells (Supplementary Fig. S4E).

To further examine the role of DAB2IP as a suppressor of cancer stemness, GFP-tagged DAB2IP-expression vector was transfected into cells and ALDH activity was determined using the Aldered assay. OC cells with high level of ectopic DAB2IP expression, marked by high GFP expression, had significantly reduced ALDH(+) population (Fig. 4A) and altered stemness characteristics, including increased sensitivity to platinum (IC_{50} from 15.63μM to 8.27μM in OVCAR3 cells; Fig. 4B) and decreased cell motility towards attractant in migration assays (Fig. 4C). Furthermore, re-expressing DAB2IP in OCSCs decreased ALDH activity (Supplementary Fig. S5A), inhibited ALDH1 expression (Supplementary Fig. S5B), decreased cell migration capacity (Supplementary Fig. S5C) and sensitized cells to cisplatin (from 62.17μM to 30.84μM CDDP; Supplementary Fig. S5D). In addition, repressed expression of genes strongly associated with stemness was observed in OCSCs re-expressing DAB2IP (Supplementary Fig. S5E). Collectively, these results indicated that DAB2IP reprogramed CSCs to a less stem-like state.

DAB2IP alters multiple cancer-associated pathways

Transcriptomic analysis of DAB2IP-overexpressing cells and empty vector control cells was carried out using RNA-sequencing and bioinformatics analysis. Altered expression of 449 genes was observed (FDR < 0.05, fold change > 2; Fig. 4D; Supplementary Table S3), including important stem cell markers (*ALDH1A1, LGR5, PROM1, TWIST1*) and ATP-binding cassette transporters (*ABCB11, ABCG1, ABCA2, ABCA3, ABCA5*), closely associated with multidrug resistance in OC (30) and other cancers (31) . Ingenuity Pathway Analysis (IPA) analysis and Gene Ontology (GO) annotations of differentially expressed genes regulated by DAB2IP revealed overlapping molecular functions and predicted the inhibition of a number of key biological processes associated with tumor progression, including cell movement of tumor cell lines, angiogenesis, development of epithelial tissue, growth of malignant tumor and synthesis of DNA (red and green circles represent up- or down-regulated genes; Fig. 4E). Moreover, gene networks revealed the potential functional impact of DAB2IP on embryonic/organismal development and organ/tissue morphology (Supplementary Fig. S6A, B), supporting a role for DAB2IP in modulating stem cell biology. Furthermore, DAB2IP overexpression altered malignancy-associated signaling pathways, including G-protein coupled receptor signaling, cAMP-mediated signaling and inhibition of matrix metalloproteases (MMPs; involving *MMP7, MMP16, MMP10*) (Supplementary Fig. S6C). These results demonstrated that DAB2IP expression induced transcriptomic changes that decreased aggressiveness of OC.

WNT5B is a direct target of DAB2IP and key regulator of OCSCs

The above differentially expressed genes were subjected to IPA to identify upstream regulators. The top upstream regulators associated with DAB2IP overexpression included mediators of the wingless-related integration site / planar cell polarity (WNT/PCP) pathway (JUN; $p= 1.15 \times 10^{-7}$) and canonical WNT/β-catenin signaling pathway (CTNNB1; p= 1.19

x 10^{-5}) (Fig. 5A). As a key role for WNT signaling in stem cell functionality has been reported (32,33), it was of interest to identify potential WNT ligands altering WNT signaling. Among the WNT family members, DAB2IP overexpression significantly ($p<0.05$) decreased WNT5B (fold change = -3.83; Supplementary Fig. S7A). Western blot analysis of DAB2IP-overexpressing cells demonstrated that expression of ALDH1 and WNT5B at the protein level were decreased (Fig. 5B). On the other hand, DAB2IP-KO increased WNT5B mRNA in OC cells (Supplementary Fig. S7B), further demonstrating that DAB2IP represses WNT5B and indicating that WNT5B contributes to the stemness phenotype. To test this possibility, OC cells were treated with recombinant WNT5B and analyzed using the Aldefluor assay. The ALDH(+) population was increased by WNT5B stimulation (Supplementary Fig. S7C). Furthermore, the addition of recombinant WNT5B reversed the anti-spheroid formation ability of DAB2IP, indicating WNT signaling pathway as a direct downstream regulator of DAB2IP (Supplementary Fig. S7D, E). Additional pathways altered by WNT5B treatment of OVCAR3 DAB2IP-overexpressing cells were then examined using reverse phase protein array (RPPA), a high-throughput antibody-based technique (34), and subsequent IPA analysis of the significantly altered proteins was performed. Pathways related to OC pluripotency were highly enriched due to WNT5B treatment (Supplementary Fig. S7F; Supplementary Table S4). Network analysis of significantly altered phospho-proteins identified top prediction score for biological processes of embryonic development, cell cycle and cell signaling (Fig. 5C). In this signaling network, C-JUN was predicted as a master regulator (Fig. 5C), indicating that WNT5B induces C-JUN activation, which was confirmed by increased nuclear phosphorylated C-JUN after recombinant WNT5B treatment (Fig. 5D, E). Moreover, based on RPPA analysis, WNT5B significantly activated C-JUN N-terminal kinase (JNK); however, phosphorylation level of β-Catenin remained unchanged (Fig. 5F, G), further demonstrating that WNT5B activates JNK/C-JUN-induced noncanonical WNT/PCP signaling.

As WNT/PCP signaling was shown to be essential for maintaining cell polarization and proper asymmetric division of stem cells (35), and previous studies have reported that JNK/C-JUN phosphorylation was due to RAC1 (36), we tested the effects of RAC1 inhibitor on reversing C-JUN phosphorylation in OC. Western blot was performed on cells transiently transfected with DAB2IP-expression vector, followed by WNT5B induction and RAC1 inhibitor NSC23766 treatment. WNT5B re-activated C-JUN phosphorylation, which was suppressed by DAB2IP-overexpression; however, this activation was suppressed by RAC1 inhibitor (Fig. 6A; Supplementary Fig. S8A), demonstrating that RAC1 inhibition prevented WNT5B-induced C-JUN activation in the absence of β-catenin or AKT activation (Supplementary Fig. S8B). In addition, of the WNT signaling inhibitors tested (IWP2 inhibitor, IWR-endo inhibitor, RAC1 inhibitor and RHO inhibitor), RAC1 inhibitor (NSC23766) was the most effective at suppressing the ALDH(+) cell population and ALDH1 expression (Supplementary Fig. S8C–E), suggesting a potential OCSC-targeted strategy.

To further investigate whether RAC1 inhibition was capable of reversing stemness caused by DAB2IP knockout, the effect of RAC1 inhibition on DAB2IP-KO cells was tested. NSC23766 treatment inhibited the increase of CD133(+) cells (Fig. 6B, Supplementary Fig. S8F) and PROM1 mRNA expression (Fig. 6C) induced by DAB2IP-KO, demonstrating that

RAC1 inhibition reversed cancer stemness downstream of DAB2IP. Furthermore, DAB2IP overexpression resulted in decreased RAC1 levels, suggesting that DAB2IP acts as a negative regulator upstream of RAC1 (Supplementary Fig. S9A). In addition, we analyzed ALDH(+) cell population after recombinant WNT5B treatment followed by RAC1 inhibitor treatment. OCSC enrichment upon WNT5B stimulation was reduced by the RAC1 inhibitor, to a level similar to RAC1 inhibitor alone (Supplementary Fig. S9B, C). To investigate the EZH2-DAB2IP-WNT5B-CJUN axis, the level of WNT5B and C-JUN activation after EZH2 inhibition was examined. EZH2 knockdown downregulated WNT5B and decreased C-JUN activation and recombinant WNT5B increased P-C-JUN in EZH2-knockdown cells (Supplementary Fig. S9D, E), suggesting WNT5B mediates EZH2 activation of C-JUN.

Inhibiting both RAC1 and EZH2 suppresses OCSC

DAB2IP upregulation represented a key vulnerability of OCSCs, but no pharmacological inhibitors of the tumor suppressor have been described. Therefore, with the goal of eradicating OCSCs, we chose to simultaneously target both upstream (EZH2 inhibitor; GSK126) and downstream (RAC1 inhibitor; NSC23766) regulators of DAB2IP. By using various doses of GSK126 and NSC23766 in combination (0–10 M and 0–100 M, respectively), synergistic inhibitory effects (CI<1) on tumorsphere survival under ultra-low attachment conditions were observed (Fig. 6D, Supplementary Fig. S9F). Furthermore, as tumorsphere size (Fig. 6E, Supplementary Fig. S9G) and OCSC population (Fig. 6F, G) were both significantly reduced by the combination treatment *in vitro*, we examined the combination treatment *in vivo.* We first performed a drug tolerability study in nude mice (n=4 NOD/SCID female mice per group). Mice were treated with GSK126 (150mg/kg, i.p.) and/or NSC23766 (2.5mg/kg, i.p.) daily (QD5) plus cisplatin (2mg/kg, i.p.) weekly for four cycles, and body weights were determined. Mice (all groups) gained weight during the treatment period (Supplementary Fig. S10A), demonstrating that the drugs were well-tolerated.

The treatment regimen was next examined in HGSOC xenograft models. Mice were injected with OVCAR3 cells (2 x 10^6 cells) s.c., and once tumor size reached 100mm^3, mice were randomized (n=6 NOD/SCID female mice per group) and treated for 4 weeks (Fig. 7A). Tumor volume was measured twice a week and the experiments were terminated one week after the last cycle of treatment (day 38 after transplantation). Although groups that received single/double drug treatment showed moderate decreases in tumor volume, those decreases were not significant compared to the vehicle control-treated group. However, the 3-drug combination (GSK126, NSC23766 and cisplatin) from day 24 onward significantly inhibited tumor volume compared to other treatments (Fig. 7B) and significantly reduced endpoint tumor weight (Fig. 7C, D). At the end of the study, tumors were harvested, dissociated to single-cell suspension for flow cytometry analysis, and the ALDH(+) population of cells was determined. The percentage of ALDH(+) cells was significantly decreased by the 3-drug combination only (Fig. 7E, Supplementary Fig. S10B).

To strengthen these observations, a second xenograft model using Kuramochi cells was established and probability of survival was assessed using the same study design. A significant increase of probability of survival was observed using combination treatment

compared to vehicle control ($P<0.01$) or NSC23766 alone ($P<0.05$) (Supplementary Fig. S10C). As proposed in Fig. 7F, inhibiting both EZH2 and RAC1 in combination with platinum chemotherapy effectively targeted the OCSC population and further decreased tumor burden compared to control or all the other single/double treatment conditions.

Discussion

OC is the deadliest gynecological malignancy in the US and more effective treatments for HGSOC are clearly needed. Toward developing new therapeutic targets for chemoresistant disease due to OCSCs, here we identify DAB2IP as an important regulator of OCSCs. We show that EZH2, the histone methyltransferase of PRC2, is responsible for epigenetic silencing of DAB2IP in OCSCs and further targeting DAB2IP reverses chemoresistance. We identify the EZH2/DAB2IP/C-JUN axis as a targetable signaling pathway to potentially eradicate OCSCs from residual tumors. We demonstrate for the first time that combining an epigenetic drug with a non-canonical WNT signaling pathway inhibitor eliminates aggressive CSC population *in vitro* and further enhances tumor reduction upon cisplatin *in vivo*. By using multiple databases, including the TCGA, we show that DAB2IP is a prognostic indicator in OC, and patient TMA data and publicly available datasets further demonstrate a significant negative correlation between EZH2/DAB2IP and patient outcome. We propose a mechanism (Fig. 7F) based on combining an epigenetic therapy with a non-canonical WNT pathway signaling pathway inhibitor to eradicate ovarian cancer stem cells and a promising strategy to prevent OC recurrence with potential for clinical translation.

While DAB2IP is an important multifunctional tumor suppressor in cancers (9,10), the role of DAB2IP in OC is limited to one study showing DAB2IP repression by a ubiquitin ligase SMURF1, resulting in altered OC cell proliferation and gain of EMT through AKT/SKP2 signaling loops (37). By using multiple approaches including ectopic overexpression and CRISPR/CAS9 knockout in a panel of OC cells, we demonstrate that DAB2IP suppression functionally maintains the phenotype and malignant potential of OCSCs, and re-expressing DAB2IP in OCSCs reprograms cells to a less stemness state. This finding is in agreement with other independent studies of renal, prostate and colorectal cancer where DAB2IP is shown to be a CSC suppressor, however through different downstream signaling pathways from our study, such as NF-κB, c-kit-PI3K-AKT-mTOR and WNT/β-catenin signaling pathway (11–13). Moreover, transcriptomic profiling and bioinformatic analysis further reveals that beyond modulating stemness-related phenotypes, DAB2IP plays previously undescribed roles in angiogenesis, cell movement, synthesis of DNA and development of epithelial tissue in OC, and functional alterations of the pathways (Supplementary Fig. S6C) may also contribute to reducing tumor malignancy in OC and other malignancies.

EZH2 maintains self-renewal of adult/embryonic stem cells, and overexpression of EZH2 can induce more differentiated cells to a pluripotent state (38,39). Here we demonstrate that spheroid formation by OCSCs is highly dependent on EZH2. Mechanistically, we show that EZH2 by suppressing DAB2IP supports OCSC maintenance and inhibiting DAB2IP in EZH2 knockdown cells rescues stemness. Our unbiased screen for EZH2/DAB2IP downstream targets reveals WNT5B-induced WNT signaling as a primary regulator downstream of DAB2IP. WNT5B is a member of the secreted WNT protein family, but how

DAB2IP regulates expression of WNT5B is unknown. Transcription factors potentially regulating WNT5B, identified by PROMO (prediction of transcription factor binding sites) analysis of the WNT5B promoter, includes the period-like domain for a DAB2IP-TRAF2 direct interaction to negatively regulate NF-κB (15), a possible mechanism underlying DAB2IP regulation of WNT5B.

WNT5B is a marker of poorly differentiated, mesenchymal-type cancer in diverse cell lines and in human tumor tissue samples (40). However, compared to other WNT ligands, the function of WNT5B remains largely unknown. Specifically, the WNT signaling pathway activated by WNT5B is unclear but likely to be cell-context specific. For example, in triple negative breast cancer, WNT5B acts through WNT/β-catenin responsive genes to modulate mitochondrial biogenesis (41), whereas in oral squamous cell carcinoma, WNT5B uses both canonical and non-canonical WNT signaling pathways to induce Snail and Slug expression (42). By utilizing RPPA to identify protein level changes upon WNT5B stimulation, we demonstrate C-JUN phosphorylation independent of WNT/β-catenin, supporting a context-dependent feature of WNT signaling pathways in different types of tissue. Although there is no reported inhibitor of WNT5B, in theory RAC1 inhibitor can be used to target WNT5B-induced C-JUN activation, which phenocopied the effect of DAB2IP. Importantly, NSC23766 in combination with the EZH2 inhibitor (GSK126) synergistically eliminated OCSC, perhaps due to reinforced inhibitory effects on the same signaling pathway. EZH2 has been shown to directly repress WNT genes, with acetylation and trimethylation exerting opposing roles on H3K27 (43,44), and inhibiting EZH2 may enhance WNT signaling unexpectedly, providing additional rationale for the greater efficacy observed using the combination treatment.

WNT/PCP signaling pathway is known to control tissue polarity and cell movement during vertebrate development, and a growing body of evidence indicates that this branch of WNT signaling is strongly implicated in cancer development at both early and late stages (45). However, compared to canonical WNT signaling pathway, WNT/PCP signaling remains incompletely understood. Correct cell polarity is responsible not only for the diversification of cell shapes, but also for regulation of the asymmetric cell divisions of stem cells, including differentiation and self-renewal (46,47). In line with this, a subset of WNT/PCP pathway genes are highly expressed in Stem-A subtype of OC, driving pluripotency and aggressiveness of tumor cells (48). Moreover, elevated expression of RAC1, an effector of WNT/PCP pathway, in OC has been reported (49). In the present study, by upregulating DAB2IP and suppressing WNT5B effects, NSC23766 in combination with GSK126 eliminates the OCSC population. Overall, we propose that targeting WNT/PCP signaling pathway components holds promise in OC treatment and warrants further investigation. In this regard, ketorolac, a pan-inhibitor of the Rho family members RAC1 and CDC42, has been tested in OC patients (49). Ketorolac confers pharmacologic activity that inhibits RAC1 and CDC42 in OC patients, potentially contributing to the observed survival benefit in women treated with the drug (49).

Clinically, OCSC targeting approaches in general remain to be firmly established. Strategies such as upfront treatment to potentially eradicate OCSCs or second-line treatment to prevent the emergence of OCSC and thus recurrent, chemoresistant disease should be strongly

considered (50). In our xenograft model, administration of OCSC-targeting therapy plus cisplatin demonstrates efficacy (e.g. inhibited tumor growth and reduced the OCSC population), supporting an approach of adjuvant treatment together with first-line therapy with the goal of improving disease-free survival. Whether tumors with low basal DAB2IP level or high EZH2 level respond better to this regimen remains to be determined. In summary, we have shown that EZH2 downregulation of DAB2IP in OCSCs results in WNT5B induced C-JUN activation. Our study for the first time demonstrates a functional role and molecular mechanisms of DAB2IP in OCSCs and provides strong rationale for targeting the EZH2/DAB2IP/C-JUN network in conjunction with platinum-based therapy in OC patients.

Supplementary Material

Refer to Web version on PubMed Central for supplementary material.

Acknowledgements

We thank Dr. Anirban Mitra (Indiana University School of Medicine) and Dr. Heather O'Hagan (Indiana University School of Medicine) for helpful discussions. We thank Christiane Hassel (Flow Cytometry Core Facility, Indiana University, Bloomington, IN) for technical assistance with flow cytometry. We thank Dr. Doug Rusch and Aaron Buechlein (Center for Genomics and Bioinformatics, Indiana University, Bloomington, IN) for help with bioinformatic analysis of RNA-seq data. We thank the Reverse Phase Protein Array (RPPA) Core (MD Anderson Cancer Center) for RPPA experiments and bioinformatics analysis. We thank the Immunohistochemical Core Lab (Indiana University School of Medicine, Indianapolis, IN) for performing immunohistochemical staining of TMA samples. This work was funded by the Congressionally Directed Medical Research Programs (CDMRP), Department of Defense, Ovarian Cancer Research Program (OCRP) Award Number W81XWh-17-1-0076, a Collaborative Research Development grant from the Ovarian Cancer Research Alliance, Van Andel Institute Stand Up To Cancer Epigenetic Therapy Dream Team (led by Dr. Peter Jones and Dr. Stephen Baylin), Medical Sciences Doane and Eunice Wright Memorial Fellowship and the Indiana Clinical and Translational Sciences Institute funded, in part by Grant Number UL1TR002529 from the National Institutes of Health, National Center for Advancing Translational Sciences, Clinical and Translational Sciences Award. The content is solely the responsibility of the authors and does not necessarily represent the official views of the National Institutes of Health.

Financial support: This work was funded by a Collaborative Research Development grant from the Ovarian Cancer Research Alliance and the Congressionally Directed Medical Research Programs (CDMRP), Department of Defense, Ovarian Cancer Research Program (OCRP) Award Number W81XWh-17-1-0076, Indiana Clinical and Translational Sciences Institute Grant Number UL1TR002529 from the National Institutes of Health, National Center for Advancing Translational Sciences, Clinical and Translational Sciences Award, Van Andel Institute-Stand Up To Cancer Epigenetics Dream Team.

References

1. Torre LA, Trabert B, DeSantis CE, Miller KD, Samimi G, Runowicz CD, et al. Ovarian cancer statistics, 2018. CA: a cancer journal for clinicians 2018;68:284–96 [PubMed: 29809280]
2. Bowtell DD, Böhm S, Ahmed AA, Aspuria P-J, Bast RC Jr, Beral V, et al. Rethinking ovarian cancer II: reducing mortality from high-grade serous ovarian cancer. Nature reviews Cancer 2015;15:668 [PubMed: 26493647]
3. Batlle E, Clevers H. Cancer stem cells revisited. Nature Medicine 2017;23:1124–34
4. Steg AD, Bevis KS, Katre AA, Ziebarth A, Dobbin ZC, Alvarez RD, et al. Stem cell pathways contribute to clinical chemoresistance in ovarian cancer. Clinical cancer research 2012;18:869–81 [PubMed: 22142828]
5. Dean M, Fojo T, Bates S. Tumour stem cells and drug resistance. Nature Reviews Cancer 2005;5:275–84 [PubMed: 15803154]

6. Zeller C, Dai W, Steele NL, Siddiq A, Walley AJ, Wilhelm-Benartzi CSM, et al. Candidate DNA methylation drivers of acquired cisplatin resistance in ovarian cancer identified by methylome and expression profiling. Oncogene 2012;31:4567–76 [PubMed: 22249249]
7. Rizzo S, Hersey JM, Mellor P, Dai W, Santos-Silva A, Liber D, et al. Ovarian cancer stem cell like side populations are enriched following chemotherapy and overexpress EZH2. Molecular cancer therapeutics 2011:molcanther. 0788.2010
8. Wang Y, Cardenas H, Fang F, Condello S, Taverna P, Segar M, et al. Epigenetic Targeting of Ovarian Cancer Stem Cells. Cancer research 2014;74:4922–36 [PubMed: 25035395]
9. Bellazzo A, Di Minin G, Collavin L. Block one, unleash a hundred. Mechanisms of DAB2IP inactivation in cancer. Cell Death Differ 2017;24:15–25 [PubMed: 27858941]
10. Liu L, Xu C, Hsieh J-T, Gong J, Xie D. DAB2IP in cancer. Oncotarget 2016;7:3766–76 [PubMed: 26658103]
11. Yun EJ, Baek ST, Xie D, Tseng SF, Dobin T, Hernandez E, et al. DAB2IP regulates cancer stem cell phenotypes through modulating stem cell factor receptor and ZEB1. Oncogene 2015;34:2741–52 [PubMed: 25043300]
12. Min J, Liu L, Li X, Jiang J, Wang J, Zhang B, et al. Absence of DAB2IP promotes cancer stem cell like signatures and indicates poor survival outcome in colorectal cancer. Scientific Reports 2015;5:16578 [PubMed: 26564738]
13. Yun E-J, Zhou J, Lin C-J, Hernandez E, Fazli L, Gleave M, et al. Targeting cancer stem cell in castration resistant prostate cancer. Clinical cancer research : an official journal of the American Association for Cancer Research 2016;22:670–9
14. Smits M, van Rijn S, Hulleman E, Biesmans D, van Vuurden DG, Kool M, et al. EZH2-Regulated DAB2IP Is a Medulloblastoma Tumor Suppressor and a Positive Marker for Survival. Clinical Cancer Research 2012;18:4048–58 [PubMed: 22696229]
15. Min J, Zaslavsky A, Fedele G, McLaughlin SK, Reczek EE, De Raedt T, et al. An oncogene-tumor suppressor cascade drives metastatic prostate cancer by coordinately activating Ras and nuclear factor-[kappa] B. Nature medicine 2010;16:286–94
16. Haley J, Tomar S, Pulliam N, Xiong S, Perkins SM, Karpf AR, et al. Functional characterization of a panel of high-grade serous ovarian cancer cell lines as representative experimental models of the disease. Oncotarget 2016;7:32810 [PubMed: 27147568]
17. Weiswald L-B, Guinebretière J-M, Richon S, Bellet D, Saubaméa B, Dangles-Marie V. In situ protein expression in tumour spheres: development of an immunostaining protocol for confocal microscopy. BMC cancer 2010;10:106- [PubMed: 20307308]
18. Wang Y, Zong X, Mitra S, Mitra AK, Matei D, Nephew KP. IL-6 mediates platinum-induced enrichment of ovarian cancer stem cells. JCI insight 2018;3
19. Tang J, Pulliam N, Özeş A, Buechlein A, Ding N, Keer H, et al. Epigenetic Targeting of Adipocytes Inhibits High-Grade Serous Ovarian Cancer Cell Migration and Invasion. Molecular Cancer Research 2018;16:1226–40 [PubMed: 29759990]
20. Fang F, Cardenas H, Huang H, Jiang G, Perkins SM, Zhang C, et al. Genomic and epigenomic signatures in ovarian cancer associated with resensitization to platinum drugs. Cancer research 2018;78:631–44 [PubMed: 29229600]
21. Chou T-C. Drug Combination Studies and Their Synergy Quantification Using the Chou-Talalay Method. Cancer Research 2010;70:440–6 [PubMed: 20068163]
22. Tan TZ, Yang H, Ye J, Low J, Choolani M, Tan DSP, et al. CSIOVDB: a microarray gene expression database of epithelial ovarian cancer subtype. Oncotarget 2015;6:43843–52 [PubMed: 26549805]
23. Bapat SA, Mali AM, Koppikar CB, Kurrey NK. Stem and progenitor-like cells contribute to the aggressive behavior of human epithelial ovarian cancer. Cancer research 2005;65:3025–9 [PubMed: 15833827]
24. Zhang S, Balch C, Chan MW, Lai H-C, Matei D, Schilder JM, et al. Identification and Characterization of Ovarian Cancer-Initiating Cells from Primary Human Tumors. Cancer Research 2008;68:4311–20 [PubMed: 18519691]

25. Landen CN, Goodman B, Katre AA, Steg AD, Nick AM, Stone RL, et al. Targeting aldehyde dehydrogenase cancer stem cells in ovarian cancer. Molecular cancer therapeutics 2010;9:3186–99 [PubMed: 20889728]
26. Silva IA, Bai S, McLean K, Yang K, Griffith K, Thomas D, et al. Aldehyde Dehydrogenase in Combination with CD133 Defines Angiogenic Ovarian Cancer Stem Cells That Portend Poor Patient Survival. Cancer Research 2011;71:3991–4001 [PubMed: 21498635]
27. Kryczek I, Liu S, Roh M, Vatan L, Szeliga W, Wei S, et al. Expression of aldehyde dehydrogenase and CD133 defines ovarian cancer stem cells. International journal of cancer 2012;130:29–39 [PubMed: 21480217]
28. Baba T, Convery P, Matsumura N, Whitaker R, Kondoh E, Perry T, et al. Epigenetic regulation of CD133 and tumorigenicity of CD133+ ovarian cancer cells. Oncogene 2009;28:209–18 [PubMed: 18836486]
29. Curley MD, Therrien VA, Cummings CL, Sergent PA, Koulouris CR, Friel AM, et al. CD133 expression defines a tumor initiating cell population in primary human ovarian cancer. Stem cells 2009;27:2875–83 [PubMed: 19816957]
30. Auner V, Sehouli J, Oskay-Oezcelik G, Horvat R, Speiser P, Zeillinger R. ABC transporter gene expression in benign and malignant ovarian tissue. Gynecologic oncology 2010;117:198–201 [PubMed: 19922990]
31. Fletcher JI, Haber M, Henderson MJ, Norris MD. ABC transporters in cancer: more than just drug efflux pumps. Nature Reviews Cancer 2010;10:147–56
32. Pattabiraman DR, Weinberg RA. Tackling the cancer stem cells – what challenges do they pose? Nature reviews Drug discovery 2014;13:497–512 [PubMed: 24981363]
33. Katoh M, Katoh M. WNT signaling pathway and stem cell signaling network. Clinical cancer research 2007;13:4042–5 [PubMed: 17634527]
34. Tibes R, Qiu Y, Lu Y, Hennessy B, Andreeff M, Mills GB, et al. Reverse phase protein array: validation of a novel proteomic technology and utility for analysis of primary leukemia specimens and hematopoietic stem cells. Molecular cancer therapeutics 2006;5:2512–21 [PubMed: 17041095]
35. Zhan L, Rosenberg A, Bergami KC, Yu M, Xuan Z, Jaffe AB, et al. Deregulation of Scribble Promotes Mammary Tumorigenesis and Reveals a Role for Cell Polarity in Carcinoma. Cell 2008;135:865–78 [PubMed: 19041750]
36. Coso OA, Chiariello M, Yu J-C, Teramoto H, Crespo P, Xu N, et al. The small GTP-binding proteins Rac1 and Cdc42regulate the activity of the JNK/SAPK signaling pathway. Cell 1995;81:1137–46 [PubMed: 7600581]
37. Fan X, Wang Y, Fan J, Chen R. Deletion of SMURF 1 represses ovarian cancer invasion and EMT by modulating the DAB2IP/AKT/Skp2 feedback loop. Journal of Cellular Biochemistry 2019;120:10643–51 [PubMed: 30672020]
38. Chang C-J, Yang J-Y, Xia W, Chen C-T, Xie X, Chao C-H, et al. EZH2 promotes expansion of breast tumor initiating cells through activation of RAF1-β-catenin signaling. Cancer cell 2011;19:86–100 [PubMed: 21215703]
39. Wei Y, Chen Y-H, Li L-Y, Lang J, Yeh S-P, Shi B, et al. CDK1-dependent phosphorylation of EZH2 suppresses methylation of H3K27 and promotes osteogenic differentiation of human mesenchymal stem cells. Nature cell biology 2011;13:87–94 [PubMed: 21131960]
40. Gujral Taranjit S, Chan M, Peshkin L, Sorger Peter K, Kirschner Marc W, MacBeath G. A Noncanonical Frizzled2 Pathway Regulates Epithelial-Mesenchymal Transition and Metastasis. Cell 2014;159:844–56 [PubMed: 25417160]
41. Yang L, Perez AA, Fujie S, Warden C, Li J, Wang Y, et al. Wnt modulates MCL1 to control cell survival in triple negative breast cancer. BMC Cancer 2014;14:124 [PubMed: 24564888]
42. Wang SH, Chang JS, Hsiao JR, Yen YC, Jiang SS, Liu SH, et al. Tumour cell-derived WNT5B modulates in vitro lymphangiogenesis via induction of partial endothelial-mesenchymal transition of lymphatic endothelial cells. Oncogene 2017;36:1503–15 [PubMed: 27593938]
43. Wang L, Jin Q, Lee J-E, Su I-h, Ge K. Histone H3K27 methyltransferase Ezh2 represses Wnt genes to facilitate adipogenesis. Proceedings of the National Academy of Sciences 2010;107:7317–22

44. Huang X, Yan J, Zhang M, Wang Y, Chen Y, Fu X, et al. Targeting epigenetic crosstalk as a therapeutic strategy for EZH2-aberrant solid tumors. Cell 2018;175:186–99. e19 [PubMed: 30220457]

45. Daulat AM, Borg J-P. Wnt/planar cell polarity signaling: new opportunities for cancer treatment. Trends in cancer 2017;3:113–25 [PubMed: 28718442]

46. Gödde NJ, Pearson HB, Smith LK, Humbert PO. Dissecting the role of polarity regulators in cancer through the use of mouse models. Experimental cell research 2014;328:249–57 [PubMed: 25179759]

47. Lee M, Vasioukhin V. Cell polarity and cancer–cell and tissue polarity as a non-canonical tumor suppressor. Journal of cell science 2008;121:1141–50 [PubMed: 18388309]

48. Asad M, Wong M, Tan T, Choolani M, Low J, Mori S, et al. FZD7 drives in vitro aggressiveness in Stem-A subtype of ovarian cancer via regulation of non-canonical Wnt/PCP pathway. Cell death & disease 2014;5:e1346 [PubMed: 25032869]

49. Guo Y, Kenney SR, Cook L, Adams SF, Rutledge T, Romero E, et al. A novel pharmacologic activity of ketorolac for therapeutic benefit in ovarian cancer patients. Clinical Cancer Research 2015;21:5064–72 [PubMed: 26071482]

50. Zong X, Nephew KP. Ovarian Cancer Stem Cells: Role in Metastasis and Opportunity for Therapeutic Targeting. Cancers 2019;11:934

Significance:

Findings show that combining an epigenetic therapy with a non-canonical WNT signaling pathway inhibitor has the potential to eradicate ovarian cancer stem cells and prevent ovarian cancer recurrence.

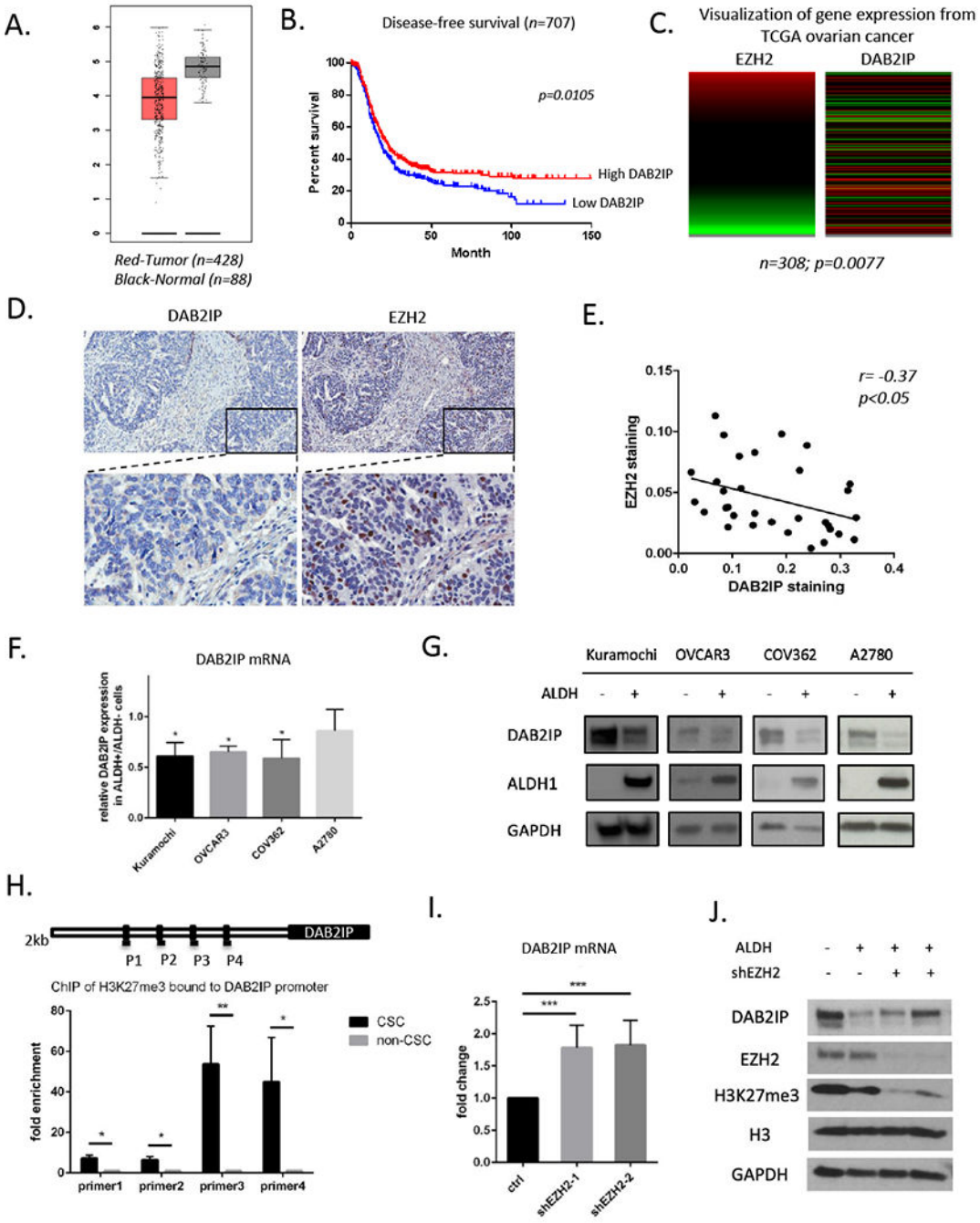

Figure 1. Low DAB2IP links to poor patient prognosis in ovarian cancer.

A) DAB2IP expression in ovarian tumor samples compared to paired normal tissues from The Cancer Genome Atlas (TCGA) data portal using Gene Expression Profiling Interactive Analysis. **B)** Kaplan-Meier survival curves of patients with high DAB2IP expression (red) and low DAB2IP expression (blue) in in Ovarian Cancer Database of Cancer Science Institute Singapore (CSIOVDB). **C)** Inverse correlation between EZH2 and DAB2IP expression at mRNA level in the ovarian cancer (OC) TCGA database. **D)** Representative pictures of immunohistochemistry (IHC) staining of DAB2IP and EZH2 on an OC tissue

microarray (TMA). **E)** An inverse correlation between EZH2 staining and DAB2IP staining is shown based on quantification of TMA analyses. **F)** DAB2IP expression was determined using quantitative real-time PCR (qPCR) in ALDH(+) cells vs. ALDH(−) cells isolated from human epithelial OC cells (Kuramochi, OVCAR3, COV362 and A2780). **G)** Western blot analysis of DAB2IP and ALDH1 in ALDH(+) vs. ALDH(−) cells isolated from human epithelial OC cells. GAPDH was used as the loading control. **H)** Enrichment of H3K27me3 at the DAB2IP promoter was quantified by qPCR after chromatin immunoprecipitation (ChIP) in ALDH(+) cells vs. ALDH(−) cells isolated from Kuramochi. **I)** DAB2IP expression was determined using qPCR in EZH2 knockdown ALDH(+) compared to ALDH(−) Kuramochi cells. **J)** Western blot analysis of DAB2IP, EZH2 and H3K27me3 in EZH2 knockdown ALDH(+) compared to ALDH(−) cells in Kuramochi. GAPDH and H3 were used as the loading controls. Representative data of at least three replicates. $P<0.05$ (*), $P<0.01$ (**) or $P<0.001$ (***).

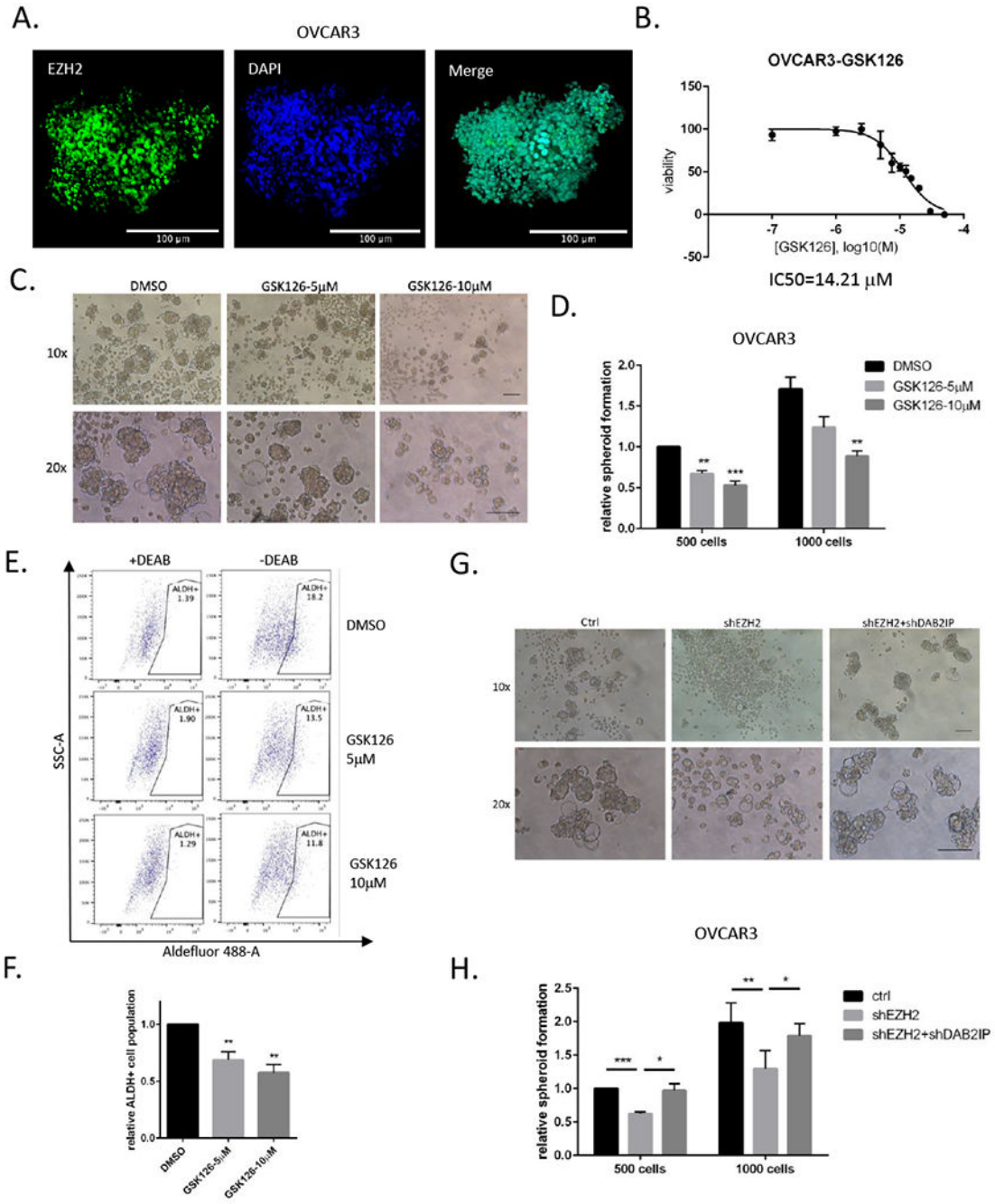

Figure 2. EZH2-regulated DAB2IP is essential for spheroid formation.

A) Immunofluorescence staining of EZH2 and DAPI in OVCAR3 spheroids **B)** IC_{50} of OVCAR3 for EZH2 inhibitor (GSK126) was determined by MTT assay. IC_{50} was determined using GraphPad. **C)** Representative images of spheroid formation (500 or 1000 OVCAR3 cells treated with GSK126 or vehicle control) in 24-well non-adherent conditions and **D)** quantification are shown. **E)** OVCAR3 spheroids were treated with GSK126 or vehicle control for 5 days. ALDH(+) cell population was determined by ALDEFLUOR assay using flow cytometry. **F)** Quantification of E). **G)** Representative images of spheroid

formation (500 or 1000 OVCAR3 cells transfected with shEZH2s, either alone or together with shDAB2IP, and control vector) and **H)** quantification are shown. Representative data of at least three replicates. Scale bar= 100μm. P<0.05 (*), P<0.01 (**) or P<0.001 (***).

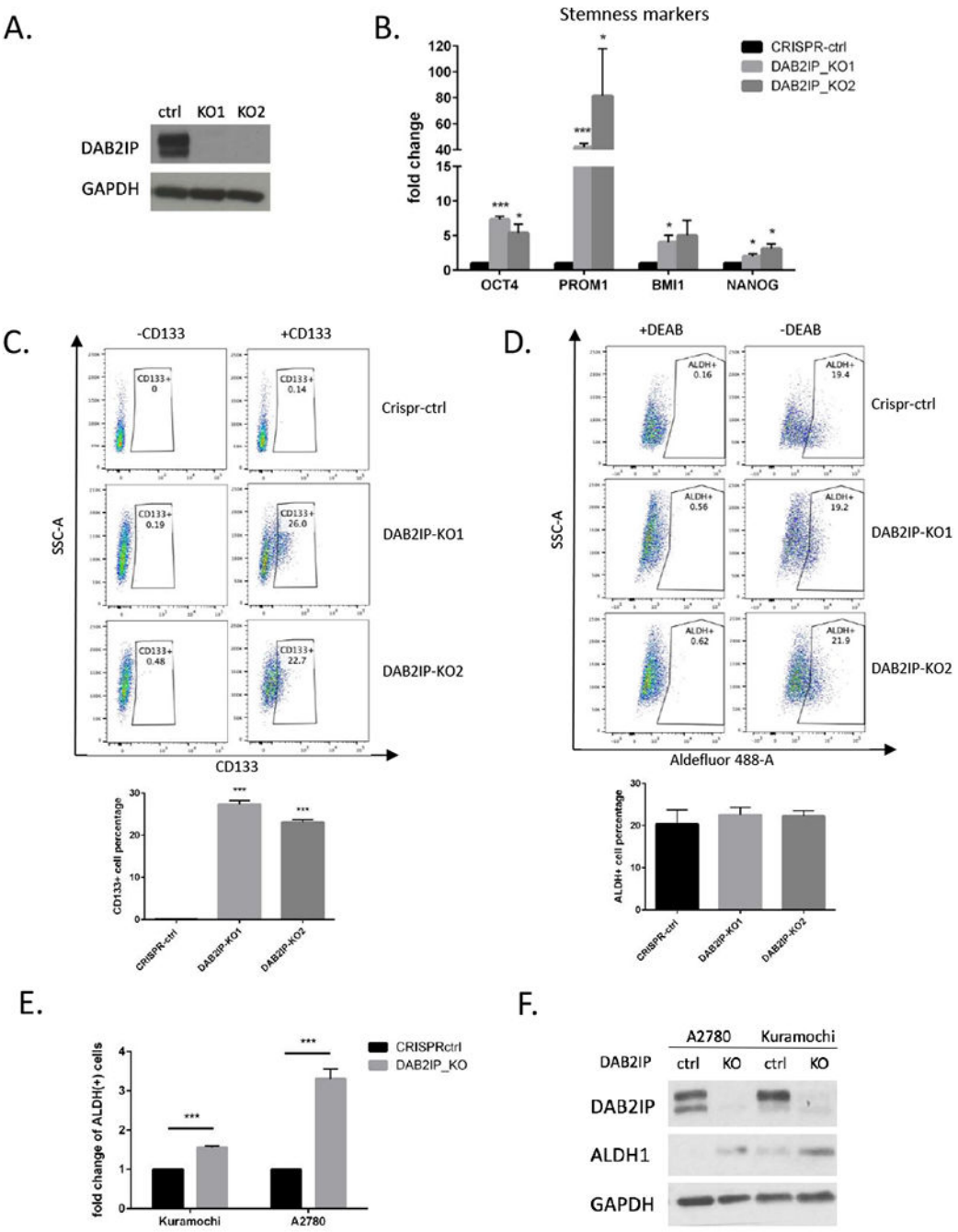

Figure 3. CRISPR knockout of DAB2IP confers cancer stemness.

A) Western blot analysis of DAB2IP in OVCAR3 DAB2IP knockout (KO) and vector control cells. GAPDH was used as the loading control. **B)** Expression of stemness-related genes was determined using qPCR in OVCAR3 DAB2IP KO vs. vector control cells. **C)** Flow cytometry analysis of CD133(+) cell population in OVCAR3 DAB2IP KO cells and vector control cells. **D)** Flow cytometry analysis of ALDH(+) cell population in OVCAR3 DAB2IP KO cells and vector control cells. **E)** Quantification of flow cytometry showing ALDH(+) cell population in Kuramochi and A2780 DAB2IP KO and vector control cells. **F)**

Western blot showing expression of DAB2IP and ALDH1 in Kuramochi and A2780 DAB2IP KO and vector control cells. GAPDH was used as the loading control. $P<0.05$ (*), $P<0.01$ (**) or $P<0.001$ (***).

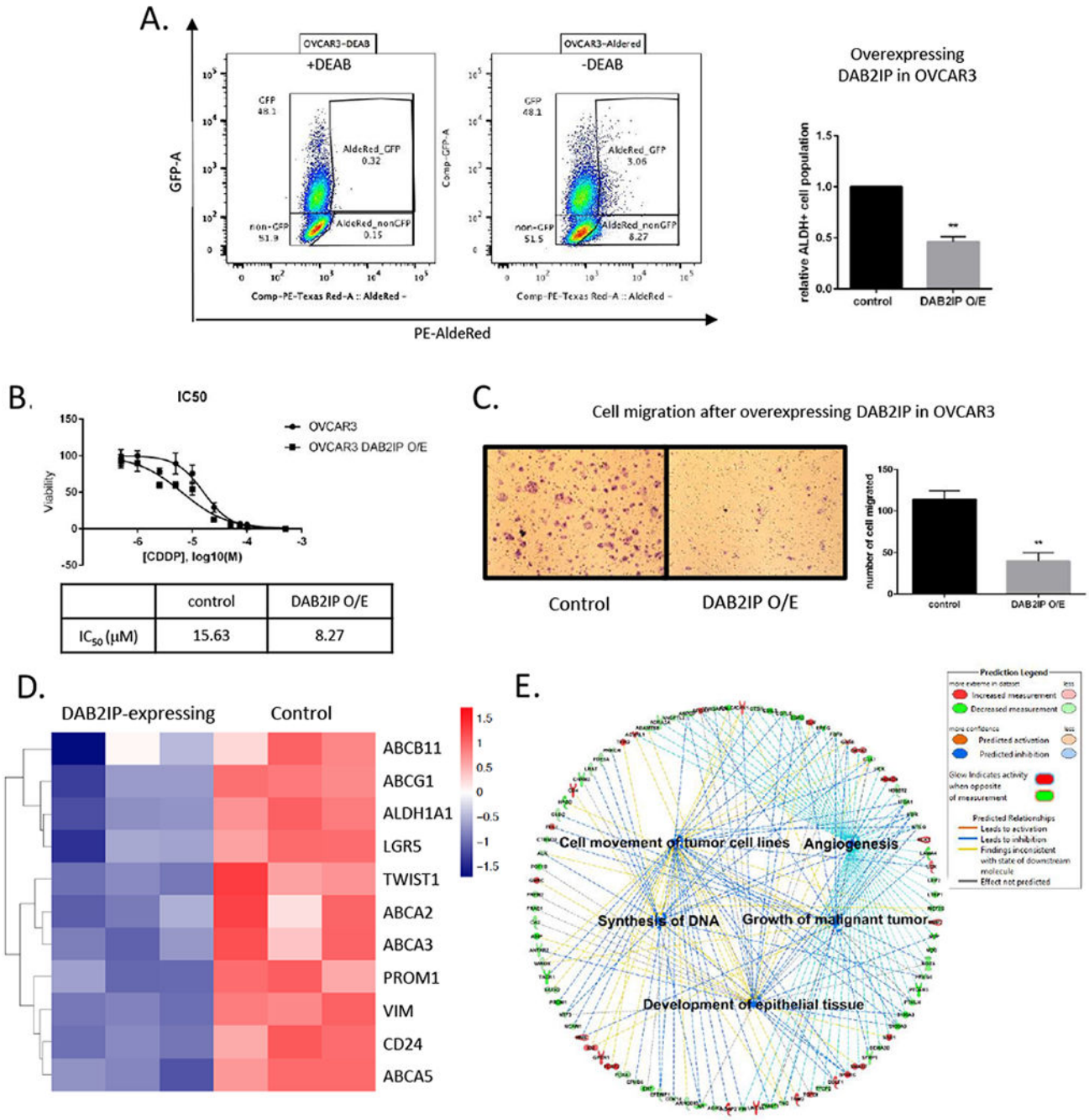

Figure 4. DAB2IP overexpression inhibits stemness phenotype in ovarian cancer cells.

A) Flow cytometry analysis showing ALDH(+) cell population in OVCAR3 DAB2IP-GFP expressing and vector control cells. **B)** The IC_{50} values for cisplatin were determined by treating OVCAR3 and OVCAR3 DAB2IP-expressing cells with increasing doses of cisplatin for 3 h, followed by a 3-day recovery and MTT assay to measure viability. IC_{50} was determined using GraphPad. **C)** OVCAR3 cells expressing empty vector and DAB2IP were seeded into migration chambers and cell migration was analyzed 16 h later. Representative images (left) and quantification (right) are shown. **D)** Heatmap of gene expression related to

stemness and ABC transporters identified by RNA-seq using OVCAR3 DAB2IP-expressing cells and control. **E)** Networks of biological processes constructed using significantly altered genes between OVCAR3 DAB2IP-expressing and control cells. Representative data of at least three replicates. $P<0.05$ (*), $P<0.01$ (**) or $P<0.001$ (***).

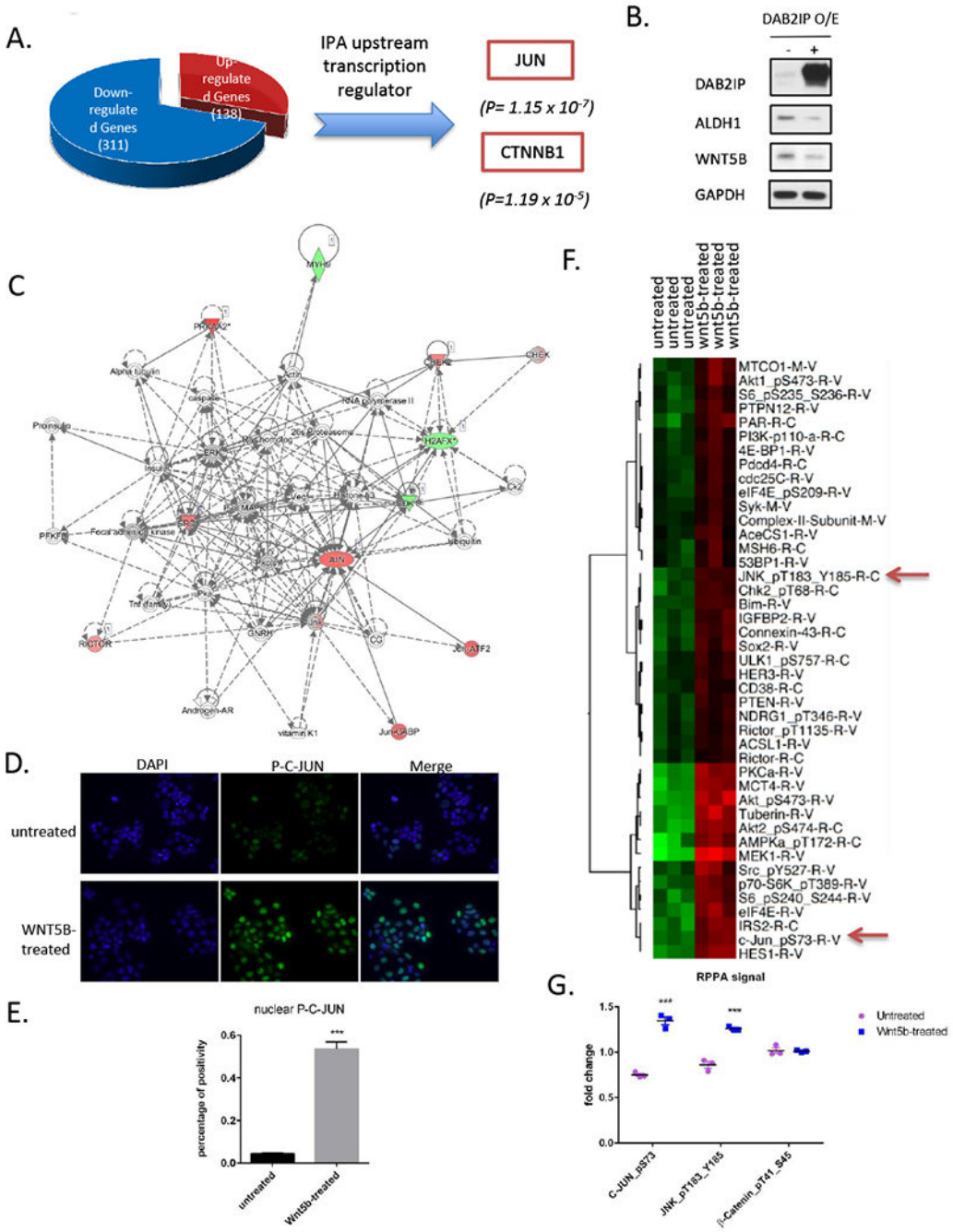

Figure 5. WNT5B-induced C-JUN activation is a direct target of DAB2IP.

A) Differentially expressed genes in control vector and DAB2IP-expressing OVCAR3 cells identified by RNA-seq were subjected to Ingenuity Pathway Analysis (IPA) for upstream regulators. **B)** Western blot analysis of DAB2IP, ALDH1 and WNT5B in DAB2IP-overexpressing and vector control cells. GAPDH was used as the loading control. **C)** Top network identified by IPA analysis of proteins significantly altered in phosphorylation status after recombinant WNT5B stimulation in Reverse Phase Protein Array (RPPA). **D)** Immunofluorescent staining of DAPI and phospho-C-JUN in OVCAR3 cells after treatment

with human recombinant WNT5B treatment for one hour. **E)** Quantification of D). **F)** Heatmap of RPPA analysis. **G)** Plotted RPPA signal for phospho-C-JUN, phospho-JNK and phospho-β-catenin. P<0.05 (*), P<0.01 (**) or P<0.001 (***).

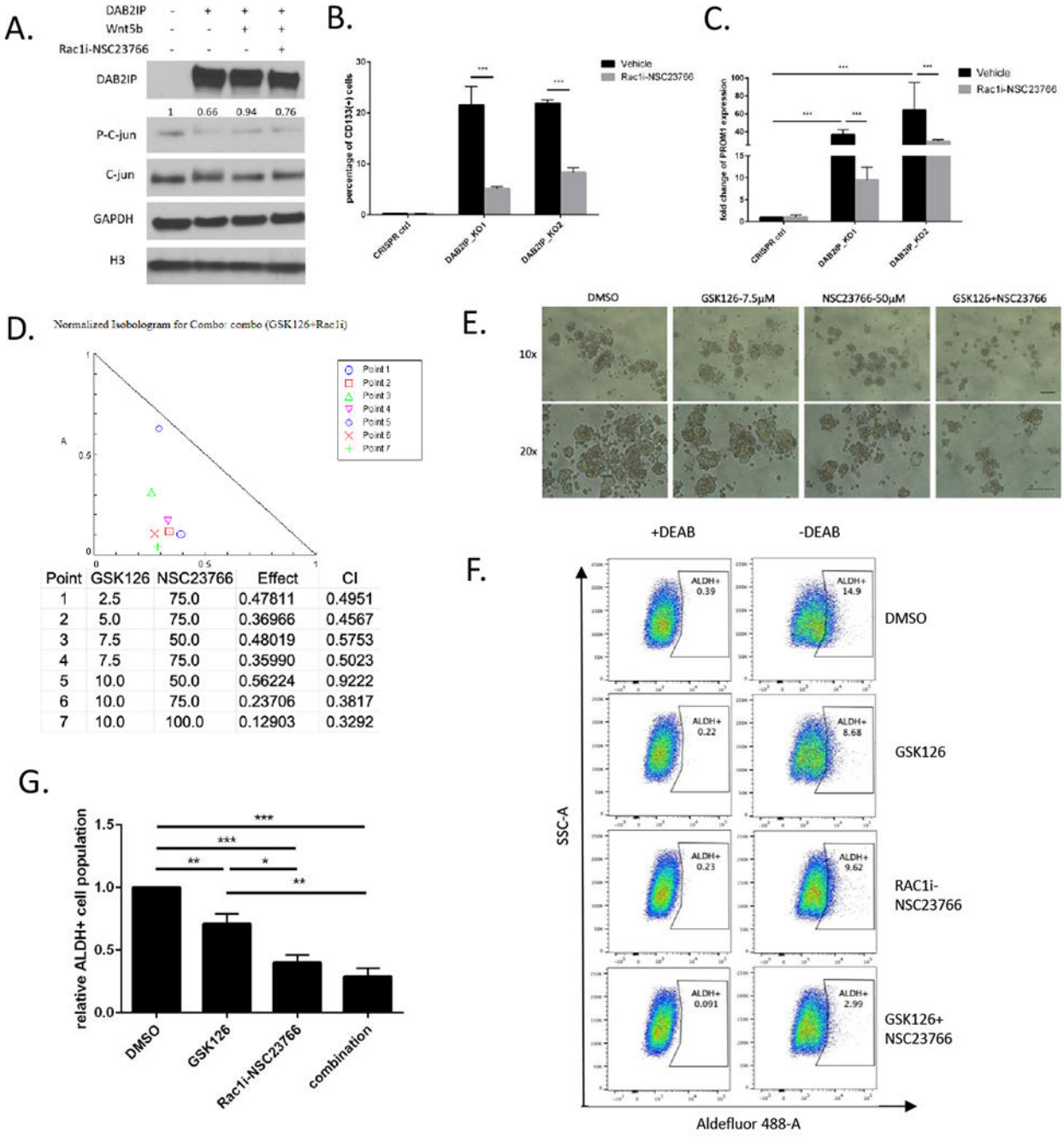

Point	GSK126	NSC23766	Effect	CI
1	2.5	75.0	0.47811	0.4951
2	5.0	75.0	0.36966	0.4567
3	7.5	50.0	0.48019	0.5753
4	7.5	75.0	0.35990	0.5023
5	10.0	50.0	0.56224	0.9222
6	10.0	75.0	0.23706	0.3817
7	10.0	100.0	0.12903	0.3292

Figure 6. Targeting RAC1 inhibits stemness phenotype and inhibiting the EZH2/DAB2IP/C-JUN axis reduces survival of OCSC.

A) Western blot analysis of DAB2IP, P-C-JUN and C-JUN in transient DAB2IP-overexpressing OVCAR3 cells treated with human recombinant WNT5B and Rac1 inhibitor (NSC23766). GAPDH and H3 were used as the loading controls. **B)** Quantification of flow cytometry showing CD133(+) population in OVCAR3 DAB2IP KO cells treated with Rac1 inhibitor (NSC23766) and vehicle control. **C)** Relative mRNA expression of PROM1 in OVCAR3 DAB2IP KO cells treated with Rac1 inhibitor (NSC23766) and vehicle control by

qPCR analysis. **D)** Normalized isobologram for combination treatment of EZH2 inhibitor (GSK126) and Rac1 inhibitor (NSC23766) at different dosages using OVCAR3 spheroids *in vitro*. **E)** Representative images of spheroid formation at day 5 are shown. **F)** Flow cytometry showing ALDH(+) cells in OVCAR3 with different treatments and **G)** quantification. Representative data of at least three replicates. Scale bar= 100μm. $P<0.05$ (*), $P<0.01$ (**) or $P<0.001$ (***).

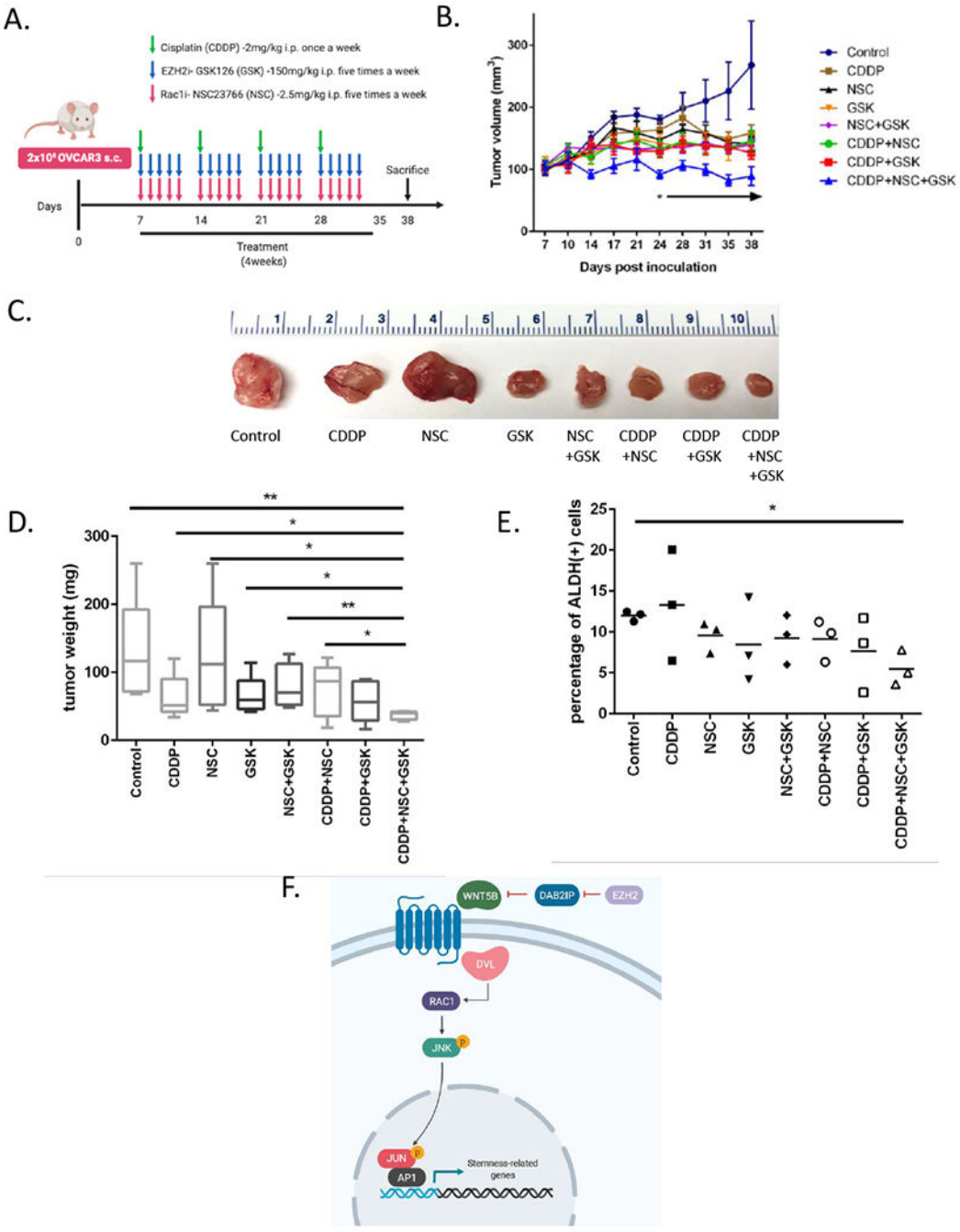

Figure 7. Combining the RAC1 inhibitor NSC23766 with the EZH2 inhibitor GSK126 inhibits tumor growth *in vivo*.

A) A diagram illustrating the experimental design including GSK126 (150mg/kg; daily-QD5) and NSC23766 (2.5mg/kg; daily-QD5), plus cisplatin (2mg/kg; weekly) followed by randomization of mice after tumor inoculation. **B)** Xenograft tumor growth curve of different treatment groups. **C)** Representative images of tumors collected at the end of the experiment. **D)** Tumor weight at the time of harvest. **E)** Quantification of flow cytometry analysis showing ALDH(+) cells in xenograft tumors from different treatment groups. **F)** A

schematic diagram of EZH2/DAB2IP/C-JUN axis signaling in OCSCs. Representative data of at least three replicates. P<0.05 (*), P<0.01 (**) or P<0.001 (***).